AIAA SciTech Forum 2026, Orlando, Florida
January 12-16, 2026

An Experimental Study of Losses in High Voltage AC Lunar Power Cables

J. Hayden Klopp,[1] George Thomas,[2] and Jeffrey Csank[3]
NASA Glenn Research Center, Cleveland, Ohio, 44135, United States

This paper describes the status of AC cable testing work that focuses on the feasibility of high frequency AC power transmission on the lunar surface. This includes assessing impacts on the power cable performance when exposed to the Lunar soil environment in the vacuum of space. Test data was recorded for power cables operating at various AC frequencies and in various environmental conditions. The testing began with an impedance sweep, and a full power transmission test in ambient conditions without any Lunar regolith simulant (to gather baseline values). After, the test setup was moved into a "dirty" thermal-vacuum (T-VAC) chamber. This chamber enabled testing in a vacuum environment with Lunar regolith simulant. The desired outcome from the testing was to determine if there was any electrical interaction between simulant and cable whether in a vacuum or ambient pressure environment. The data recorded in vacuum and in the ambient environment were not significantly different, allowing additional testing to be completed in ambient conditions. Additional test configurations were completed with the cable coiled along the surface, buried within the simulant, and entirely separated from the simulant with no major discernable losses measured. Frequency selection also did not alter the test data.

I. Introduction

NASA's Artemis campaign is focused on returning human Astronauts to the Moon, establishing a permanent presence where Astronauts can stay on the Moon for up to 30 days, and learn in preparation for Mars. While the first two Artemis missions don't involve landing on the Moon, human presence on the Moon is currently planned to resume with the Artemis III mission. NASA will also make history by exploring the Lunar South Pole [1]. Subsequent Artemis missions will focus on establishing a permanent presence on the Moon and will require the development of a power architecture that is functional in a Lunar environment and enables ubiquitous, universal access to reliable electrical power to accomplish this goal.

Power cabling for the lunar surface must be both lightweight and capable of operating in an unforgiving thermal and radiation environment. To reduce cable mass and improve efficiency (driven by the resistive losses of the cable), it is desired to increase the voltage. For high voltage DC power transmission systems, there is a current upper limit around 1200 to 1500 V. This limit is attributed to radiation hardening of power electronics and limit of the number of DC-to-DC converters needed in series to reach higher voltages balances against overall reliability. Designs including such large numbers of series stages pose prohibitive reliability concerns. DC-to-AC converters can be made with a single power stage to produce any desired AC output voltage using transformers, resulting in rugged, highly reliable designs. The conclusion gathered from the early research was that 3000 VAC, 3 phase, 1000 Hz is the best choice considering transmission system mass and efficiency, for a large power transmission grid [2]. One limitation of an AC power system, however, is the selection of the frequency of the power transmitted to maximize overall system performance.

The frequency selection will impact the selection of the converters, transformers, generators, and transmission lines used in the power transmission system. 1000 Hz was seen as a promising candidate [2], but testing to explore the possible unintended consequences of the frequency selection had not been conducted. One possible unintended consequence to the frequency choice is inductive and/or capacitive coupling between the Lunar regolith and the power

[1] Electrical Engineer, Power Management and Distribution Branch, jeffrey.h.klopp@nasa.gov
[2] Electrical Engineer, Power Management and Distribution Branch, george.l.thomas@nasa.gov
[3] Electrical Engineer, Power Management and Distribution Branch, jeffrey.t.csank@nasa.gov , AIAA Sr. Member

transmission cabling. The wireless energy transfer to the Lunar regolith could pose a hazard for astronauts and become a major power loss mechanism. The severity of these losses was hypothesized to be inversely proportional to frequency, and moreover, that the losses exceed 5% at frequencies less than 400 Hz for 1 km transmission distance. This is referred to as the hypothesis throughout the remainder of this document.

NASA's Moon-to-Mars objectives [3] and especially its objective to produce (and inevitably transmit) 100 kW of power via its planned fission surface power (FSP) asset [4] necessitates testing to confirm or reject this hypothesis in order to derisk the required power management technologies.

This paper discusses completed research at NASA Glenn Research Center focused on better characterizing power cable performance in a terrestrial and simulated Lunar environment. Section 2 describes the test plan and the selected Lunar regolith simulant. Section 3 provides the results from the testing. Finally, Section 4 offers some concluding remarks.

II. Test Plan

To better understand the loss mechanisms due to inductive and/or capacitive coupling between the cable and lunar regolith, a series of tests were performed in both in atmospheric pressure testing and in vacuum testing within a thermal-vacuum (T-VAC) chamber. Test variables in this campaign included the cable design (the device under test or DUT), as well as the environment that the cable was tested in. At each test point in the test matrix, an impedance sweep (defined further in Section II. A), and a full power test (defined further in Section II B.) were performed.

Selection of the appropriate Lunar regolith simulant was critical because of the variance in electrical properties found in commercially available simulants. The Lunar Regolith Simulant User's Guide [5], as well as feedback provided by the NASA Lunar Surface Innovation Initiative's (LSII's) Simulant Advisory Committee [6], was instrumental in determining the proper simulant. Magnetic susceptibility in the simulant was one of the primary attributes of concern. The magnetic susceptibility could be artificially increased by adding olivine, ilmenite, or another additive with iron oxide in it. While making the simulant more magnetically susceptible, this idea wasn't implemented because of the concern that it would change how similar the simulant is to actual Lunar regolith. Another simulant attribute that influenced our selection was what region of the Moon the simulant was attempting to replicate. The Lunar South Pole is the target of this work due to it being the destination of the Artemis missions and its potential to provide access to ice and other mineral resources [7]. Thus, the regolith simulant replicating the mare region of the Moon was most appropriate. Finally, as physical distribution can be related to electrical properties, simulant minerology and particle distribution were also considered. The simulant selected with all these considerations in mind was the JSC-1A simulant. JSC-1A rated well for the specific characteristics of interest (magnetic susceptibility, grain size, etc) and replicates the mare region of the Moon. A large quantity of JSC-1A was available for testing, and about 173 kg of simulant was poured into the soil bin.

A. Impedance Sweep

To gather impedance data versus frequency, both short circuit (measuring resistive and inductive parts of the cable impedance) and open circuit tests (measuring the capacitive part) are conducted at each test point. The short circuit test and open circuit test configurations are shown in Fig. 1 and Fig. 2 respectively. In both types of tests, the frequency response analyzer generates a sine wave from 10 to 100,000 Hz, and the output is connected through a linear amplifier to the cable under test. In the short circuit test, the amplifier output and test probes are connected between the input conductor of interest (e.g., Phase A) and ground (e.g., Phases B and C as well as the shield or ground conductor shorted together). All conductors on the output side of the cable are shorted to ground. This test pushes the perturbation current through the phase conductor of interest and measures its impedance, which generally follows a series RL circuit. This allows estimation of the resistance and inductance parameters of the cable. The open circuit test, which captures line-to-ground capacitance information, is conducted the same as the short circuit test, but disconnects the phase of interest (e.g., Phase A) at the output side of the cable so that current must flow capacitively from the phase of interest, through the other cable conductors, to ground. An example of an impedance Bode chart collected in this work is shown in Fig. 3.

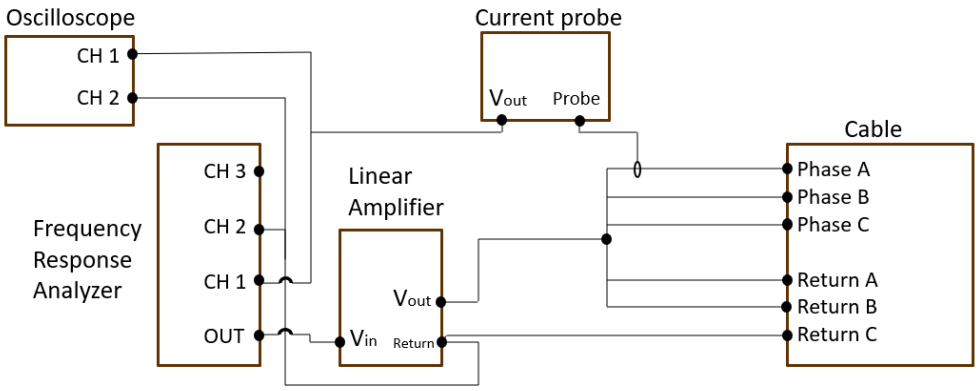


Fig. 1. Block diagram of resistive/inductive coupling test (short circuit test).

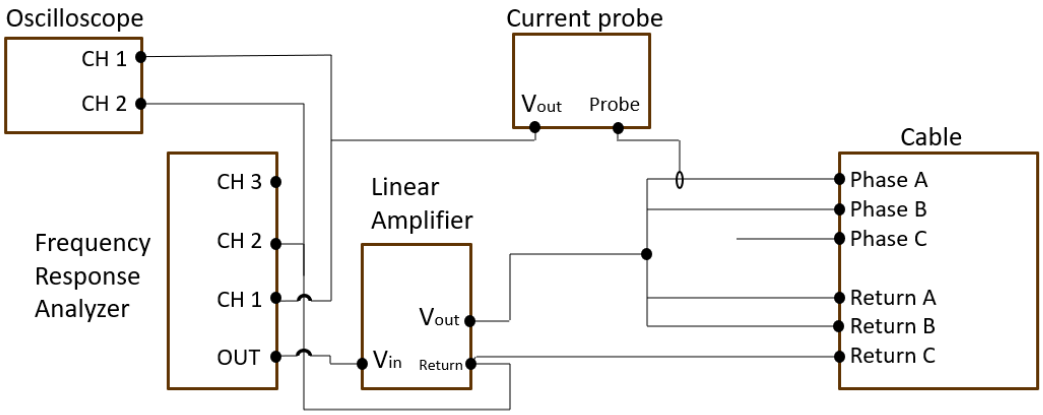


Fig. 2. Block diagram of capacitive coupling test (open circuit test).

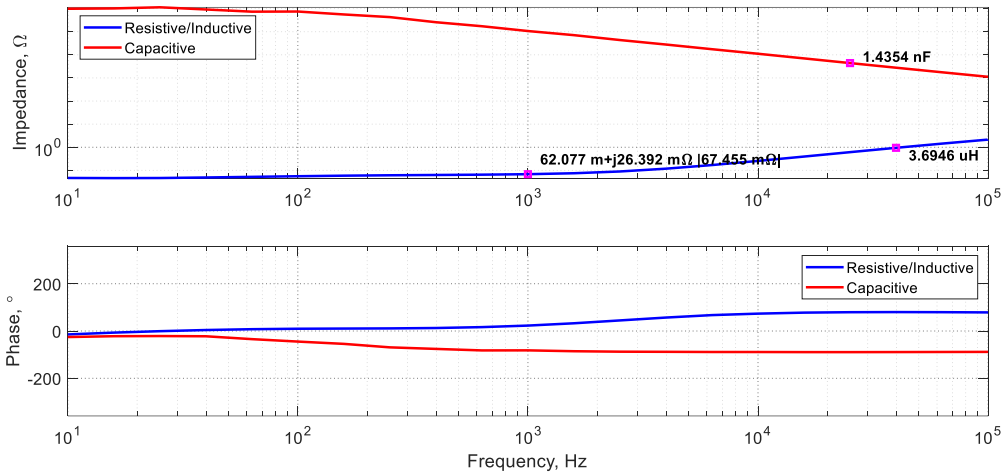


Fig. 3. Example impedance bode chart from the baseline shielded cable test.

B. Full Power Transmission Test

The full power transmission test was performed by feeding 3000 $V_{L\text{-}L}$ to the cable via a programmable 3-phase AC power supply and set of off-the-shelf medium voltage step up transformers wired Wye-Wye. A resistive load included in a rack along with the step-up transformers was used to draw 2.5 kW through the cable. The selection of

voltage aligns with the conclusions determined from previous studies, but the frequency was modified to determine its impact on the losses in the cable DUT. The power test was performed at 60, 100, 400, 800, 1000, and 1500 Hz. These selected frequencies span the research space that was investigated in previous work for AC Lunar power systems [2]. The AC Power Supply produced approximately 208 V_{L-L} which was fed into the transformer bank, which then scaled the voltage up to 3000 V_{L-L} AC. The cable was next routed through the soil bin for testing, and back out to the load. Between the power supply and load, an oscilloscope and power analyzer were connected (visually depicted in Fig. 4). The power was measured at the input and output sides of the cable, and the difference provided an estimate of the power losses.

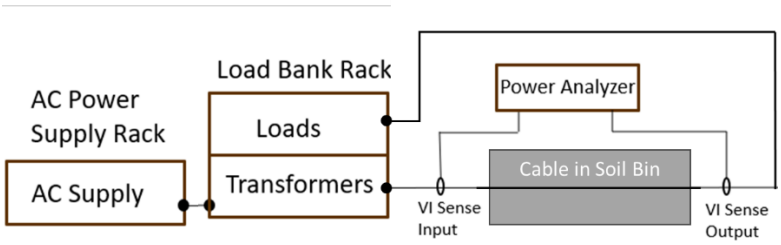


Fig. 4. Block diagram of full power transmission test.

C. Cable Configuration

One variable explored in this test campaign is the cable (i.e., the DUT). The first cable (Test Cable 1) used for testing was a jacketed three conductor cable fabricated to power, voltage, and frequency specifications by a US vendor. The cable was 25 feet in length, and contained 12-gauge conductors with a 20-gauge drain wire. The cable was insulated with Ethylene Tetrafluoroethylene (ETFE) which allowed the cable to operate with 3000 V_{L-L} AC (5200 V AC peak). The first cable was incorporated in early testing and testing under vacuum, with the shielding providing protection for a Lunar environment. The second cable (Test Cable 2), produced in-house, was an unshielded cable with three power conductors and a ground conductor. The cable was 25 feet in length and all four conductors were 18-gauge chosen as the only high voltage wire readily available to the testing team. The cable was insulated with silicone, enabling operating voltage of up to 10,000 V DC. The second cable was tested in the ambient pressure environment as guided by the findings from the shielded cable testing. A third test cable (Test Cable 3) was made of the same material as the first cable but was fabricated to the minimum possible length that can connect the input and output terminals of the load bank rack (approximately six inches). It functioned as a control test case for the cable configuration variable and was primarily used to estimate instrument error in the other test cases.

D. Environmental Configuration

The environmental configuration variable explored in this test campaign represents the materials in proximity to the cable. This includes the atmosphere seen by the cable (ambient pressure and hard vacuum), as well as the solid materials the cable is in contact with. The solid material configurations include 1) the cable sitting on a nonconductive floor used as a baseline, 2) the cable laying across the JSC-1 regolith simulant, 3) the cable buried in simulant, 4) cable touching regolith at two discrete contact points, 5) the cable laying in the empty, grounded aluminum soil bin, and finally, 6) the cable resting on a plastic cover above the bin, which eliminates the opportunity for capacitive and inductive coupling between the bin and the cable and is essentially a repeat of material configuration 1).

E. Test Matrix

A graphical representation of the entire suite of tests performed is given in the test matrix in Table 1. The remainder of this section describes the individual tests within this matrix in greater detail.

Table 1. Test matrix used in the test campaign.

Environmental Material Configuration	Test Cable 1 (Shielded Cable)	Test Cable 2 (Unshielded Cable)
1) Cable on nonconductive floor	0: Ambient	—
2) Cable laying across regolith	1: Vacuum / 2: Ambient	5: Ambient
3) Cable buried in regolith	3: Ambient	6: Ambient
4) Cable touching regolith twice	4: Ambient	7: Ambient
5) Cable laying in empty bin	8: Ambient	9: Ambient
6) Cable isolated in bin	10: Ambient	11: Ambient

Configuration 0 (Baseline): Test Cable 1 laid across nonconductive raised floor

Before beginning the testing work in earnest, an initial baseline test point was run to provide data to compare to the various other tests. The cable was laid on a raised floor with tiles composed of engineered wood with a laminate surface veneer, which should not interact electrically with the cable. The impedance sweep and full power tests were run. No photos or diagrams of this configuration are given due to its simplicity.

Configuration 1: Test Cable 1 laid across simulant under vacuum

The first test conducted was a vacuum test with the cable laying across the regolith simulant. Temperature inside the chamber was not controlled. An impedance sweep and full power transmission test were performed under these conditions. A camera was installed inside the tank which could capture possible eruptions in the simulant bin caused by gasses trapped in the simulant suddenly escaping. Within the resolution of the camera (which was 2 MP resolution at 120 FPS), no such simulant disturbance was noticed. Note that no eruption, arcing, or other deleterious condition was detected by the camera or other instruments throughout this test. Chamber pressure of 9e-6 Torr was maintained at all times throughout the active testing phase. A photo and diagram of the test configuration are given in Fig 5.

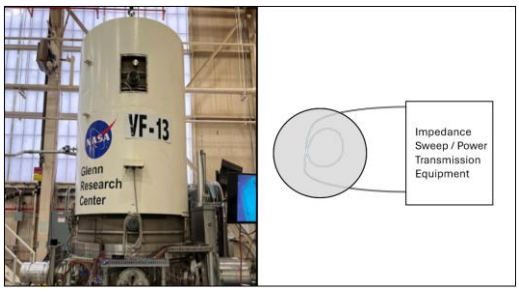


Fig 5. Configuration 1 picture and diagram.

Configuration 2: Test Cable 1 laid across simulant

The second configuration was run with the same cable configuration after the tank was vented to atmospheric pressure and the lid was removed. An impedance sweep and full power transmission test were performed under these conditions. This configuration is shown in Fig 6.

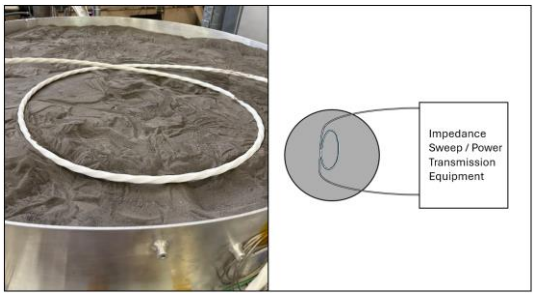


Fig 6. Configuration 2 picture and diagram.

Configuration 3: Test Cable 1 buried in simulant

In this configuration, Test Cable 1 was buried in the bin. An impedance sweep and full power transmission test were performed under these conditions. This configuration is shown in Fig 7.

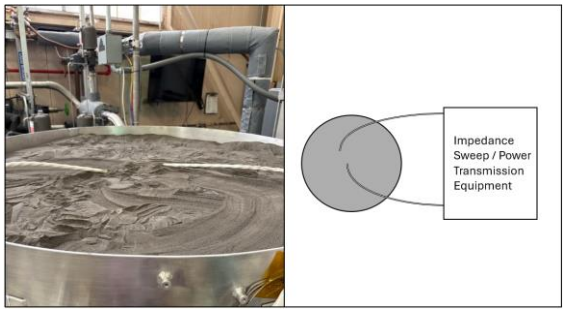


Fig 7. Configuration 3 picture and diagram.

Configuration 4: Test Cable 1 with two contact points with simulant

The soil bin in the fourth figuration contained regolith simulant, and the Test Cable 1 was suspended such that it touched the simulant at two contact points (marked with red Xs in Fig 8). An impedance sweep and full power transmission test were performed under these conditions.

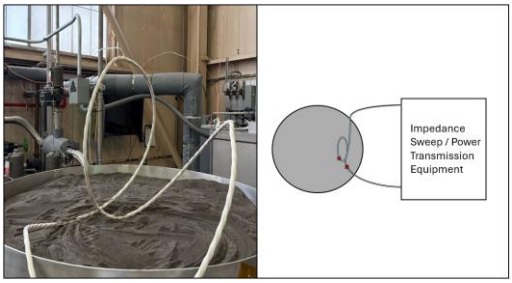


Fig 8. Configuration 4 picture and diagram.

Configuration 5: Test Cable 2 laid across simulant

The soil bin in the fifth configuration contained regolith simulant, and the Test Cable 2 was laid across the bin. An impedance sweep and full power transmission test were performed under these conditions. This configuration is shown in Fig 9.

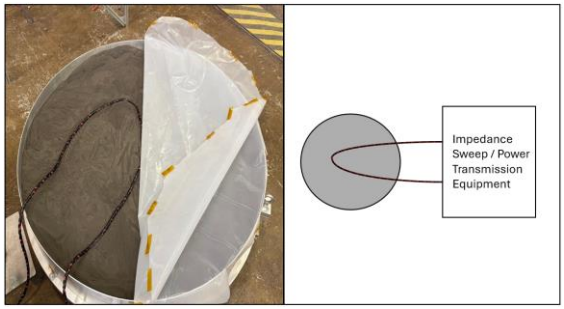


Fig 9. Configuration 5 picture and diagram.

Configuration 6: Test Cable 2 buried in simulant

The soil bin in the sixth configuration contained regolith simulant, and the Test Cable 2 was buried in the bin. The cable was buried in three inches of regolith simulant. An impedance sweep and full power transmission test were performed under these conditions as shown in Fig 10.

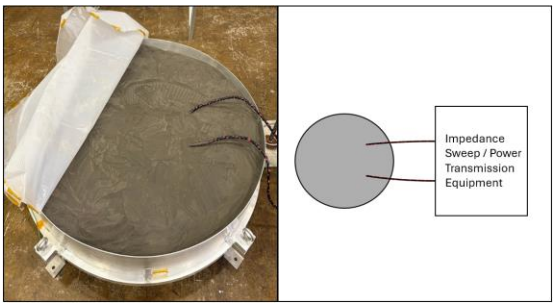


Fig 10. Configuration 6 picture and diagram.

Configuration 7: Test Cable 2 with two contact points with simulant

The soil bin in the seventh figuration contained regolith simulant, and the Test Cable 1 was manipulated to only touch the simulant at two contact points (marked with red Xs in Fig 11). An impedance sweep and full power transmission test were performed under these conditions.

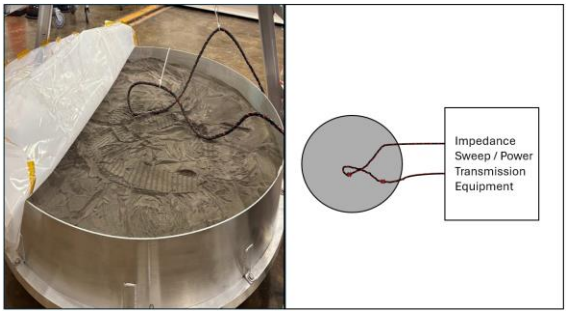


Fig 11. Configuration 7 picture and diagram.

Configuration 8: Test Cable 1 in soil bin without simulant

The soil bin in the eighth configuration did not contain regolith simulant, and the Test Cable 1 was laid across the bin. An impedance sweep, and full power transmission test was performed under these conditions. This configuration is shown in Fig 12

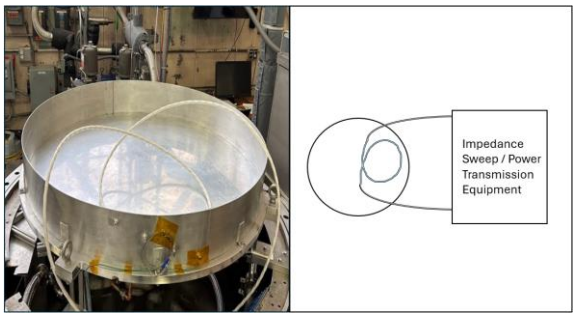


Fig 12. Configuration 8 picture and diagram.

Configuration 9: Test Cable 2 in soil bin without simulant

The soil bin in the nineth configuration did not contain regolith simulant, and the Test Cable 2 was laid across the bin. An impedance sweep, and full power transmission test was performed under these conditions. This configuration is shown in Fig 13

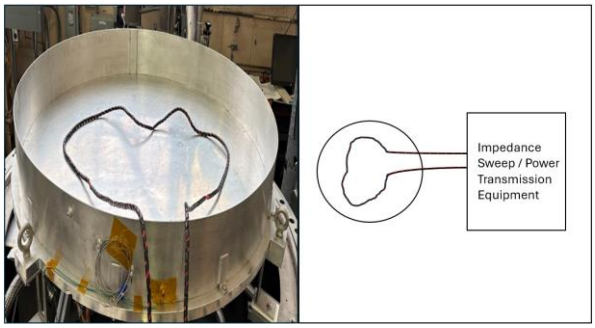


Fig 13. Configuration 9 Picture and Diagram

Configuration 10: Test Cable 1 electrically isolated in bin

The soil bin in the tenth configuration did not contain regolith simulant, and the Test Cable 1 was electrically isolated in the bin. A 3/4 inch plastic sheet material was placed between the bin and the cable to achieve isolation. An impedance sweep, and full power transmission test was performed under these conditions. No photo or diagram is given as this is essentially a repeat of configuration 0.

Configuration 11: Test Cable 2 electrically isolated in bin

Configuration 11 was the same as configuration 10 but with the Test Cable 2 used as the DUT instead of Test Cable 1. An impedance sweep, and full power transmission test was performed under these conditions. No photo or diagram is given as this is essentially a repeat of configuration 0.

Configuration 12: Test Cable 3 outside of bin

The soil bin in the twelfth configuration was not used. The Test Cable 3 was connecting directly from input to the output of the test equipment. An impedance sweep, and full power transmission test was performed under these conditions. No photo or diagram of this configuration is given as it represents a configuration with a minimally short cable DUT to obtain data to estimate measurement error.

III. Test Results

Three visualizations are provided to analyze the test results. Fig 14 shows the impedance data collected for all shielded cable test cases plotted versus frequency with the short circuit test data in blue solid lines, and open circuit data in red dashed lines. Purple markers are drawn on datapoints where resistance, capacitance, and inductance are calculated looking left to right. Specific values are also indicated on the figure. Fig 14 shows each test with the shielded cable plotted on top of one another to analyze the variation of the impedance parameters from test to test. Note that there is no obvious pattern to this variation for resistive impedance, which is about 50% worst case. The lack of pattern suggests that the variation in losses as predicted by the impedance data does not correlate to the test configuration, providing one datapoint suggesting that the loss mechanisms hypothesized are not seen in this data. The variation could be due to systematic variation (e.g., change in how the cable is geometrically laid out from test to test) or due to random error.

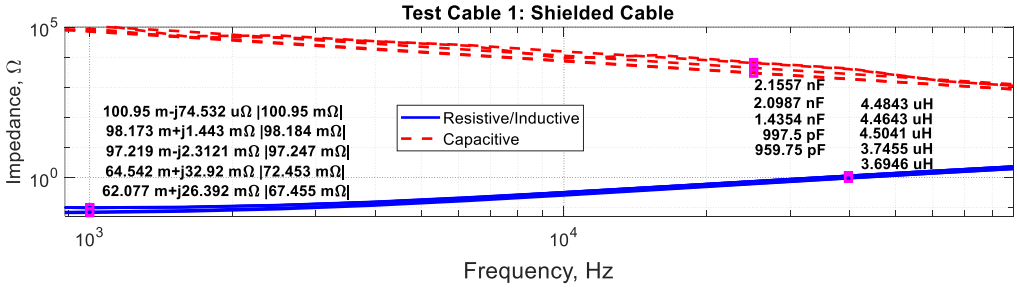


Fig 14. Impedance Bode plot data for all shielded cable test cases.

A similar plot in Fig 15 shows the impedance data from the unshielded test cases. It shows more variation from test to test in the impedance parameters (closer to 200% worst case variation), but otherwise shows the same trends as the shielded cable. This suggests (inconclusively) that the unshielded cable's impedance may be more sensitive to variations in how the cable is laid out or other uncontrolled differences from test-to-test. These differences are not correlated with the amount of contact that the cable has with the regolith simulant or other surfaces (conductive or non-conductive).

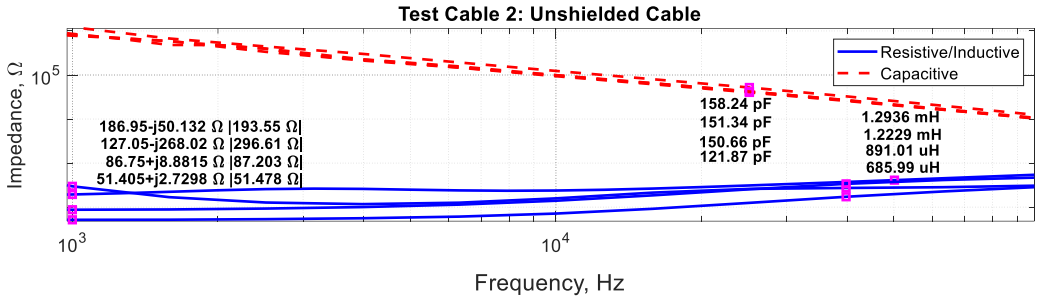


Fig 15. Impedance Bode plot data for all unshielded cable test cases.

Fig 16 shows power test losses data for a variety of shielded and unshielded tests—the legend makes reference to the particular test configuration number as defined in Section II.E. Note that tests 8, 9, 10, and 11 are omitted, as these used a different instrumentation configuration that estimated the power losses to be around 10 W, similarly to the other datasets, but showed trends that are scattered and inconsistent with the other data.

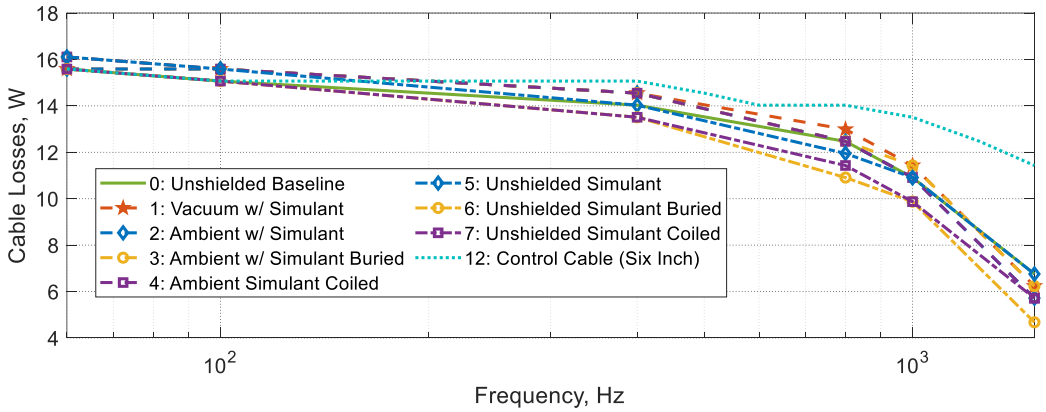


Fig 16. Power loss data computed by the power test instrumentation.

The key takeaway from Fig 16 is that the loss appears to decrease as frequency is increased, in agreement with the hypothesis. However, the losses seen in this data are all within the 1% accuracy of the instruments used to capture the voltage and current data which were ultimately used to compute power loss. For scale, note that the power transmitted in this test is 2500 W, and the losses reported by the power analyzer are at most 16 W. These losses are very low, approximately 0.64% of the power transmitted. In fact, the real cable losses are likely lower than those shown here. This is apparent when one compares the losses in tests 0 through 7 with the losses in test 12 (the control test) which generally follow each other, though with an increasing deviation at and above 1 kHz. It is also apparent when one compares these losses to those that can be calculated based on the impedance measured in the impedance sweep tests.

The cable resistance is predicted by the impedance sweep tests to be within 60 to 200 mΩ. Note that the impedance test results were computed with calibrated instruments and that they agree well with resistance measurements reported by a calibrated digital multimeter. The losses, P_{Loss}, seen from 2.5 kW of power flowing through the impedance test's reported resistance can be computed as I^2R losses where the current, I, can be computed as

$$I = \frac{P}{3\frac{V_{LL}}{\sqrt{3}}} = \frac{2500\ \text{W}}{3\frac{3000\ \text{V}}{\sqrt{3}}} = 0.48113\ \text{mA} \quad (1)$$

P_{Loss} then is computed as 0.48^2 mA^2 times 60 to 200 mΩ which equals somewhere in the range of 16 to 55 mW. This is around 3 orders of magnitude less than that predicted by the power test instrumentation. This suggests a gross overestimation of the losses by the power analyzer used in the full power test. While the actual power loss values reported by this instrument are not useful at these low levels, the lack of significant variation in them is useful information. Given that there is no significant variation from test to test in this power loss data, it suggests that no loss mechanism is detectable within the accuracy of the instruments used in the test.

IV. Conclusion

The data from this test campaign show no detectable loss mechanism for 25 ft runs of cable in any of the environments or cables tested. There was some variation in resistive and capacitive impedance among the different cable and test configurations, but none of the tests measured significant power losses or indications of losses due to capacitive or inductive coupling between the cable and the regolith. Additional tests can be performed using Lunar regolith simulants with other unique characteristics (such as the MLS-1 with higher magnetic susceptibility [3]). The interaction between the cable and Lunar regolith simulant is being characterized to publish useful scientific information to promote the ability of US industry and international partners to develop and deploy technologies for Lunar surface power. These technologies promise to enable a Lunar power system that is permanent, reliable, and extensible.

For future work, the accuracy of the instrumentation setup should be improved. Measuring losses in highly efficient systems is a problem that is known to be highly challenging. Some approaches involve calorimetry (measuring the temperature rise or heat dissipation due to the I^2R losses in the DUT instead of electrical-based measurements [8]. Another approach is to increase the length of the cable, and thus increase the losses (theoretically linearly). The authors expect the second approach of running similar tests with much longer cables to be promising, however the facilities to run 100s to 1000s of meters of cable in the presence of a simulant with high electrical and magnetic fidelity do not currently exist.

Acknowledgments

The authors thank NASA's Space Technology Mission Directorate for funding this work, and specifically thank Jenna Fothergill, the project manager responsible for this work, and Soravud (Joe) Piboontum, the program element manager responsible for it. The authors would also like to thank Anthony Colozza for describing previously unpublished work that attempted to model loss mechanisms related to capacitive and inductive coupling between AC power cables on the Moon and the Lunar regolith environment. Finally, the authors thank the facilities engineering and technician team who operated the T-VAC tank, fabricated the test hardware, and performed other critical work including Sean Hewlett, Peter Minidis, Don Fong, Casey Theman, Dave Hausser, the late Mingo Rolince, and others.

References

[1] National Aeronautics and Space Administration, "Artemis III: NASA's First Human Mission to Lunar South Pole," 13 January 2023. [Online]. Available: https://www.nasa.gov/missions/artemis/artemis-iii/.

[2] G. Thomas, "A Modular AC to DC Interface Converter to Enable Lunar Surface Power Transmission," in *Energy & Mobility Technology, Systems, and Value Chain Conference & Expo* , Cleveland, OH, 2023.

[3] National Aeronautics and Space Administration, "Moon-to-Mars Architecture Definition Document (ESDMD-001 Rev-B MD-01)," April 2025.

[4] S. Duffy, "Directive on Fission Surface Power (FSP) Development," 4 August 2025. [Online]. Available: https://www.nasa.gov/wp-content/uploads/2025/08/nasa-fsp-directive-aug42.pdf. [Accessed 26 November 2025].

[5] A. S. e. al., "Lunar Regolith Simulant User's Guide Revision A," NASA, Houston, 2024.

[6] National Aeronautics and Space Administration, "ARES | Exploration Science Projects | Lunar Regolith Simulants | Simulant Advisory Committee," 27 November 2025. [Online]. Available: https://ares.jsc.nasa.gov/projects/simulants/advisory-committee.html.

[7] National Aeronautics and Space Administration, "NASA's Plan for Sustained Lunar Exploration and Development 1," 01 August 2020. [Online]. Available: https://www.nasa.gov/wp-content/uploads/2020/08/a_sustained_lunar_presence_nspc_report4220final.pdf. [Accessed 15 September 2025].

[8] D. Christen,, U. Badstuebner, J. Biela and J. W. Kolar, "Calorimetric Power Loss Measurement," in *The 2010 International Power Electronics Conference*, Sapporo, Japan, 2010.